Ore Geology Reviews 58 (2014) 41–54

Contents lists available at ScienceDirect

Ore Geology Reviews

journal homepage: www.elsevier.com/locate/oregeorev

Zinc, sulfur and lead isotopic variations in carbonate-hosted Pb–Zn sulfide deposits, southwest China

Jia-Xi Zhou [a,b,c,*], Zhi-Long Huang [a], Mei-Fu Zhou [b], Xiang-Kun Zhu [c,**], Philippe Muchez [d]

[a] State Key Laboratory of Ore Deposit Geochemistry, Institute of Geochemistry, Chinese Academy of Sciences, Guiyang 550002, PR China
[b] Department of Earth Sciences, The University of Hong Kong, Hong Kong, PR China
[c] Laboratory of Isotope Geology, MLR, State Key Laboratory of Continental Dynamics, Institute of Geology, CAGS, Beijing 100037, PR China
[d] Geodynamics and Geofluids Research Group, KULeuven, Celestijnenlaan 200E, B-3001 Heverlee, Belgium

ARTICLE INFO

Article history:
Received 21 May 2013
Received in revised form 2 September 2013
Accepted 31 October 2013
Available online 13 November 2013

Keywords:
Zn–S–Pb isotopic variations
Sphalerite
Country rocks
Sources of metals and sulfur
Carbonate-hosted Pb–Zn sulfide deposits
Southwest China

ABSTRACT

The Sichuan–Yunnan–Guizhou Pb–Zn metallogenic province in the western Yangtze Block, southwest China, contains more than four hundred Pb–Zn deposits with more than 200 million tons of Pb–Zn ores at mean grades of 5 wt.% Pb and 10 wt.% Zn. These deposits are hosted in Sinian (Ediacaran) to Permian carbonate rocks and are structurally controlled by thrust fault–fold structures, and are spatially associated with the late Permian ~ 260 Ma Emeishan flood basalts. Two representative low temperature hydrothermal Pb–Zn sulfide deposits, the Tianqiao and Banbanqiao deposits in the southeastern part of the Sichuan–Yunnan–Guizhou Pb–Zn metallogenic province are selected for Zn–S–Pb isotopic analyses. Sphalerite from the Tianqiao deposit has δ^{66}Zn values ranging from −0.26 to +0.58‰ relative to the JMC 3–0749L zinc isotope standard, whereas δ^{66}Zn values of sphalerite from the Banbanqiao deposit range from +0.07 to +0.71‰. The zinc isotopic composition of sphalerite from both deposits increase from early to final mineralization stage. In addition, sphalerite from the center (near to bottom) part of the No. 1 ore body in the Tianqiao deposit has lower δ^{66}Zn values (−0.01 to +0.43‰) than those (+0.11 to +0.57‰) in the periphery (near to top). Sinian to Permian sedimentary rocks and Permian Emeishan flood basalts, the potential zinc metal source rocks, have δ^{66}Zn values range from −0.24 to +0.17‰ and from +0.32 to +0.44‰, respectively. The majority of the hydrothermal sphalerite has heavier zinc isotope than the country rocks, precluding the mixing of multiple zinc sources as the key factor controlling the spatial and temporal variations of zinc isotope. Therefore, the increased δ^{66}Zn values from the early to late stage and from the center to top could be due to kinetic Raleigh fractionation. Sphalerite from the Tianqiao and Banbanqiao deposits has δ^{34}S values ranging from +10.9 to +14.8‰ and from +3.9 to +9.0‰, respectively, lower than Cambrian to Permian marine sulfates (+15 to +35‰) and sulfate-bearing evaporates (+15 to +28‰) in the Devonian to Permian carbonate host rocks. Sulfur of the Pb–Zn ores from both deposits is interpreted as the result of thermal chemical sulfate reduction of evaporates in the sedimentary rocks, most likely the host rocks. Sphalerite from the Tianqiao deposit has Pb isotope similar to that of age-corrected Devonian to Permian carbonate host rocks, whereas sphalerite from the Banbanqiao deposit has Pb isotope similar to that of age-corrected underlying Precambrian basement rocks. Therefore, at least lead in the Tianqiao and Banbanqiao deposits was mainly originated from the host rocks and the underlying basements, respectively. Zn–S–Pb isotopic studies of sphalerite from both deposits indicate that sources of metals and sulfur in the hydrothermal fluid for the Tianqiao deposit are the Paleozoic carbonate host rocks, whereas for the Banbanqiao deposit the sources are the Precambrian basements and the Paleozoic carbonate host rocks, respectively.

© 2013 Elsevier B.V. All rights reserved.

1. Introduction

Recent advances in multiple collector inductively coupled plasma mass spectrometry (MC-ICP-MS) allow the analysis of the isotopic compositions of transition metals (such as Cu, Zn and Fe) from hydrothermal ore deposits (e.g., Fernandez and Borrok, 2009; Fujii et al., 2011; Gagnevin et al., 2012; Haest et al., 2009; Ikeihata and Hirata, 2012; Larson et al., 2003; Maréchal et al., 1999; Markl et al., 2006; Mason et al., 2005; Mathur et al., 2009, 2010, 2012; Rouxel et al., 2004; Wang et al., 2011; Zhu et al., 2000, 2002). Of these, the zinc isotope system has seen an increasing interest as a potential tool for understanding geochemical processes of zinc transportation and deposition in hydrothermal systems (Gagnevin et al., 2012; John et al., 2008; Kelley et al., 2009; Mason et al., 2005; Toutain et al., 2008). Studies suggest that three main processes can be used to explain variations of

* Correspondence to: J.-X. Zhou, State Key Laboratory of Ore Deposit Geochemistry, Institute of Geochemistry, Chinese Academy of Sciences, Guiyang 550002, PR China. Tel.: +86 851 5895900; fax: +86 851 5891664.
** Corresponding author.
E-mail addresses: zhoujiaxi@vip.gyig.ac.cn (J.-X. Zhou), xkzhu0824@gmail.com (X.-K. Zhu).

0169-1368/$ – see front matter © 2013 Elsevier B.V. All rights reserved.
http://dx.doi.org/10.1016/j.oregeorev.2013.10.009

zinc isotope during precipitation: kinetic Raleigh fractionation (Gagnevin et al., 2012; John et al., 2008; Kelley et al., 2009; Maréchal and Sheppard, 2002; Wilkinson et al., 2005), temperature gradient (Mason et al., 2005) and mixing of multiple zinc sources (Wilkinson et al., 2005). However, the evolutions of zinc isotope in hydrothermal deposits and the most important controlling factors are still unclear.

In the western Yangtze Block, SW China, the Sichuan–Yunnan–Guizhou Pb–Zn metallogenic province hosts over 400 Pb–Zn deposits with more than 200 million tons (Mt) of P–Zn ores grading 5 wt.% Pb and 10 wt.% Zn, making it one of the world's largest Pb–Zn producers (Deng et al., 2000; Hu and Zhou, 2012; Liu and Lin, 1999; Zhou et al., 2013a, 2013b). This metallogenic province contains several world-class deposits, such as the Huize Zn–Pb–Ge–Ag deposit (Han et al., 2007; Zhou et al., 2001) and the Daliangzi Zn–Pb–Cd deposit (Zheng and Wang, 1991). The deposits are hosted in Sinian (Ediacaran) to Permian carbonate rocks and are structurally controlled by thrust fault–fold structures and are spatially associated with the late Permian ~ 260 Ma mantle plume-derived Emeishan flood basalts (Han et al., 2007; Huang et al., 2010; Liu and Lin, 1999; Zhou et al., 2001, 2002a, 2011). Previous studies focused on the geology and origin of these deposits (e.g., Deng et al., 2000; Han et al., 2004, 2007, 2012; Huang et al., 2003, 2010; Li et al., 2007a, 2007b; Zheng and Wang, 1991; Zhou et al., 2001, 2011, 2013a, 2013b, 2013c) demonstrating that those deposits differ from the type of magmatic hydrothermal,

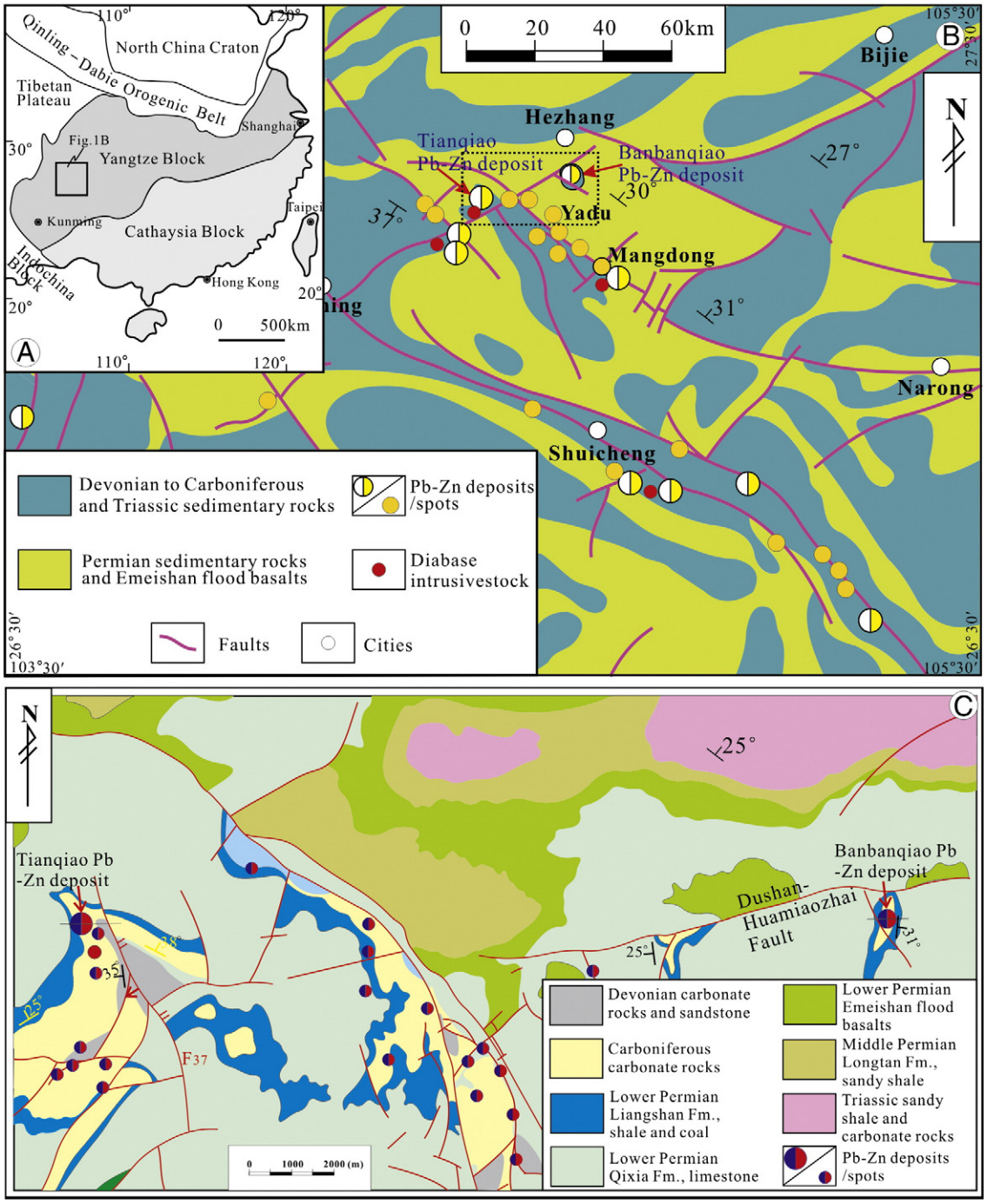

Fig. 1. The Sichuan–Yunnan–Guizhou Pb–Zn metallogeinc province is located in the western Yangtze Block, southwest China (A); geological map of the southeastern part of the Sichuan–Yunnan–Guizhou Pb–Zn metallogeinc province (modified from Zhou et al., 2011) shows the strata, faults and distribution of Pb–Zn deposits (B); geological map of the Tianqiao to Banbanqiao Pb–Zn deposits shows distributions of Devonian to Triassic sedimentary rocks, late Permian Emeishan flood basalts, structures and Pb–Zn deposits (C).

volcanic-hosted massive sulfides (VHMS), sedimentary exhalative (SEDEX) and typical Mississippi valley-type (MVT) deposits (e.g., Han et al., 2007; Zhou et al., 2013a).

This paper reports the first zinc isotope data for two representative Pb–Zn deposits, the Tianqiao and Banbanqiao deposits in the southeastern part of the Sichuan–Yunnan–Guizhou Pb–Zn metallogenic province, southwest China. Using the zinc isotope data in combination with sulfur and lead isotopes of sphalerite from both deposits and country rocks including Sinian to Permian sedimentary rocks and Permian Emeishan flood basalts, the possible controls on the zinc isotopic variations during Pb–Zn mineralization and sources of metals and sulfur are discussed.

2. Geological setting

2.1. Regional geology

The Yangtze Block is composed of ~2.9 to ~3.3 Ga crystalline basement complexes (Gao et al., 2011; Qiu et al., 2000), Meso- to Neo-Proterozoic folded basements and Paleozoic to Mesozoic cover sequences (Sun et al., 2009; Wang et al., 2010, 2012; Yan et al., 2003; Zhao et al., 2010). The folded basements include the ~1.7 Ga Dongchuan and ~1.0 Ga Kunyang Groups and equivalents rocks (Sun et al., 2009; Zhao et al., 2010). The sedimentary sequences consists of well-bedded greywackes, slates and carbonaceous to siliceous sedimentary rocks

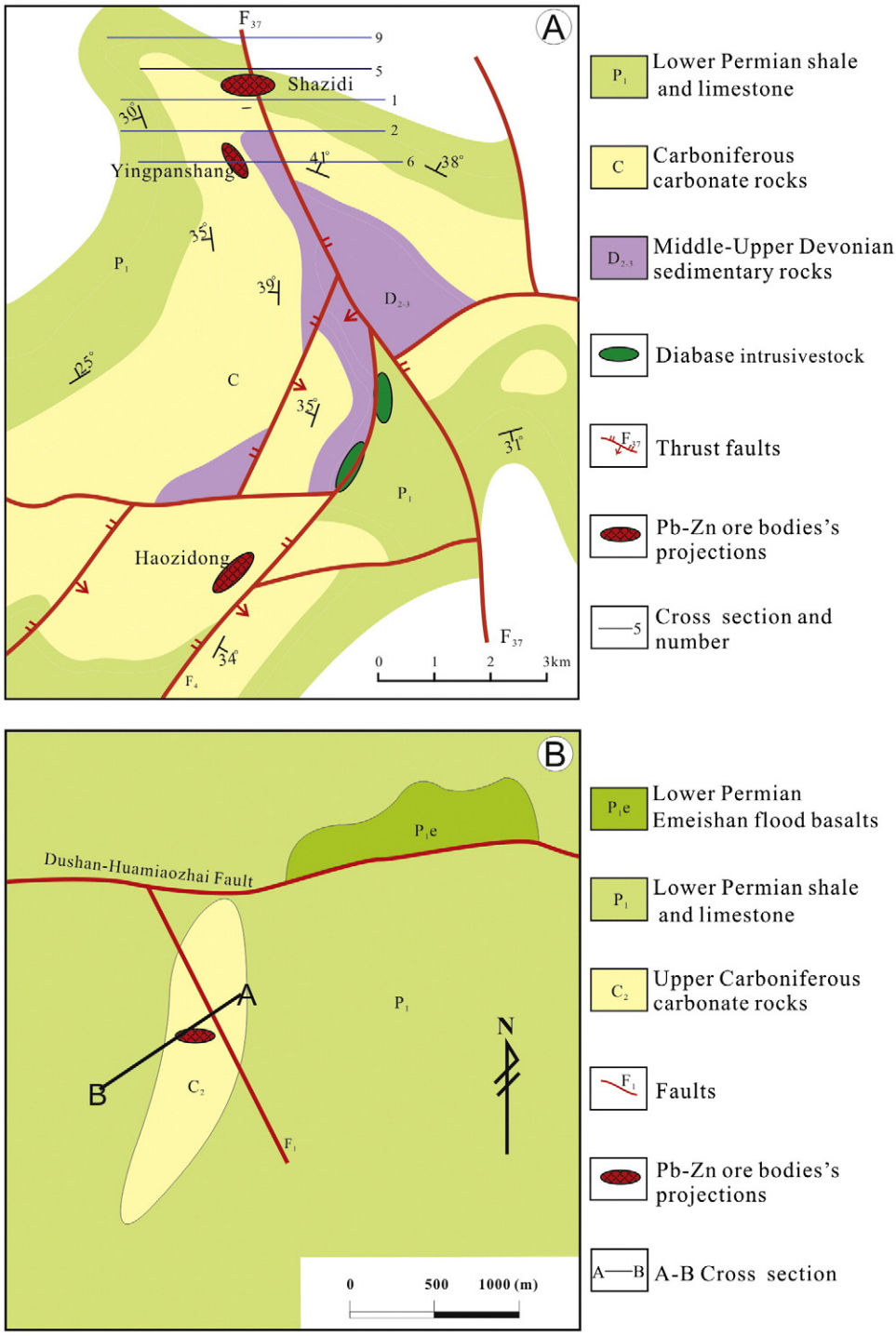

Fig. 2. Geological maps of the Tianqiao (A) and Banbanqiao Pb–Zn deposits (B) show the distribution of strata, lithologies, structures, diabase intrusivestocks and ore bodies's projections.

that are tightly folded but only weakly metamorphosed and intruded by abundant Neo-Proterozoic mafic–ultramafic and felsic intrusions (Zhou et al., 2002a). The Paleozoic to Mesozoic shallow marine cover sequences are widely distributed and include Cambrian strata of black shale, sandstone and limestone inter-bedded with dolostone, Ordovician sequences of thick-bedded limestone interlayered with dolostone and argillaceous siltstone, Lower–Middle Silurian shale and fine-grained sandstone and Devonian to Triassic sedimentary rocks. Sulfate-bearing evaporates occur widespread in the Cambrian to Triassic sedimentary rocks (Han et al., 2007; Liu and Lin, 1999). The Jurassic to Cenozoic strata are entirely continental in origin (Han et al., 2007; Zheng and Wang, 1991; Zhou et al., 2001, 2011).

In the western Yangtze Block, southwest China, the late Permian ~ 260 Ma Emeishan Large Igneous Province is cover an area of more than 250,000 km^2 (e.g., Chung and Jahn, 1995; Zhou et al.,

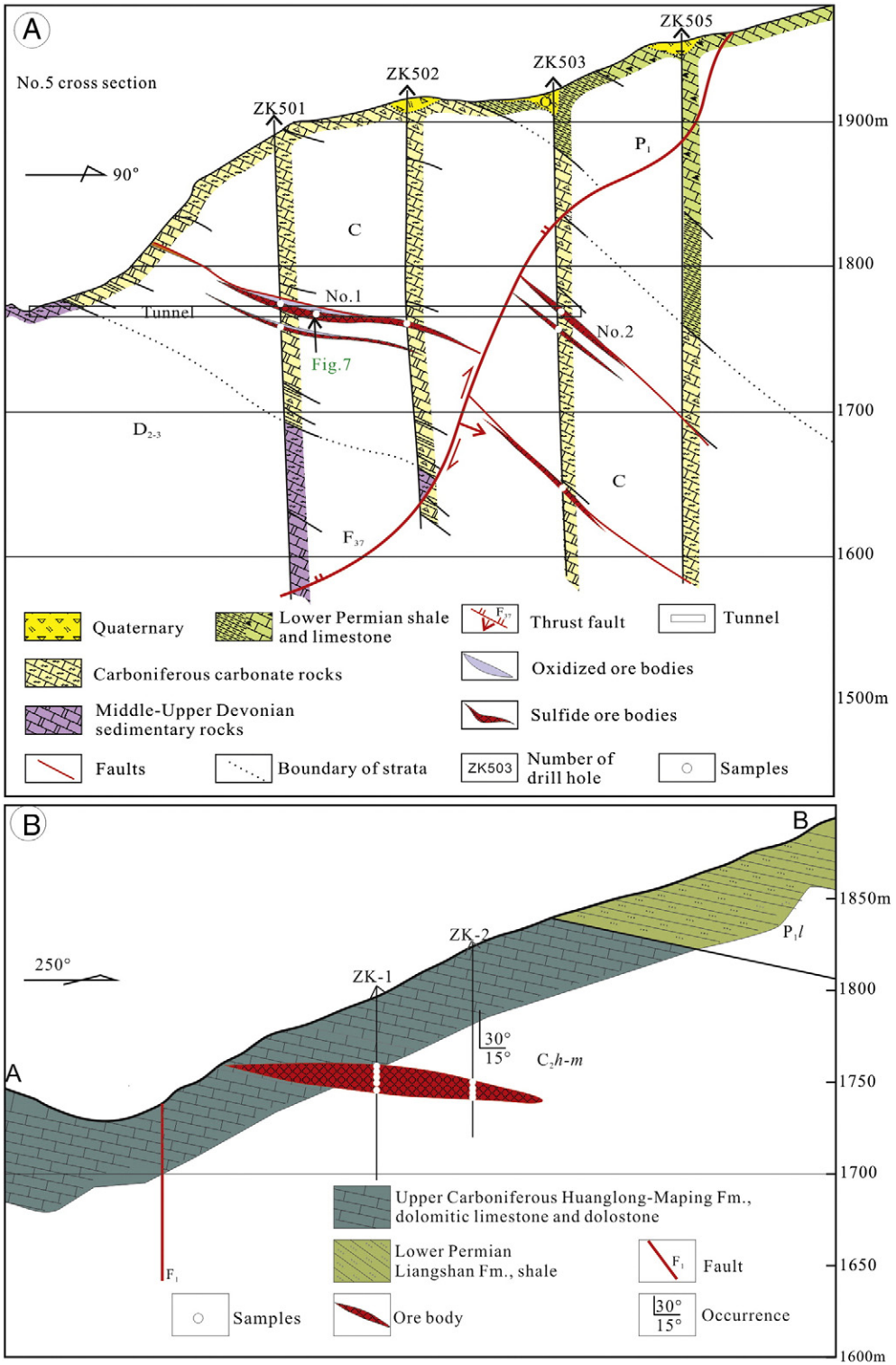

Fig. 3. The No. 5 cross section of the Tianqiao Pb–Zn deposit shows the occurrences of ore bodies, host rocks, faults and the sample's locations (A); cross section of the Banbanqiao Pb–Zn deposit shows the ore body shapes and host rocks and the sample's locations (B).

2002b). This igneous province is dominantly composed of volcanic rocks known as Emeishan flood basalts. During the Triassic–Jurassic (~200 Ma), the Yangtze Block was collided with adjacent geological bodies (such as the Yidun Arc), resulting in the closure of the Tethys Ocean (e.g., Han et al., 2012; Reid et al., 2007; Zhang et al., 2006; Zhou et al., 2013a). This event is known as the Indosinian Orogeny and caused the formation of thrust faults and folding strata (e.g., Han et al., 2012; Zhou et al., 2013c).

Over 400 Pb–Zn deposits in the western Yangtze Block are distributed in a large triangular area of 170,000 km^2 in NE Yunnan, NW Guizhou and SW Sichuan provinces (e.g., Han et al., 2007; Zheng and Wang, 1991; Zhou et al., 2001, 2011). These deposits are hosted in Paleozoic to Mesozoic carbonate rocks, which are all overlain by the Permian Emeishan flood basalts (Han et al., 2007; Huang et al., 2010; Zhou et al., 2013a). Faults in the western part of the metallogenic province trend NS and NE (Han et al., 2007; Zhou et al., 2013c), whereas NW-trending faults are dominant in the eastern part (Fig. 1B; Zhou et al., 2013a). Distribution of the Pb–Zn deposits is structurally controlled by these faults (e.g., Han et al., 2007; Liu and Lin, 1999; Zhou et al., 2013c).

2.2. Geology of the southeastern Sichuan–Yunnan–Guizhou Pb–Zn metallogenic province

In the southeastern part of the Sichuan–Yunnan–Guizhou Pb–Zn metallogenic province, the cover sequence is Devonian to Triassic in ages (Fig. 1B). Both Devonian and Carboniferous strata consist of sandstone, siltstone, limestone and dolostone. The early Permian sedimentary sequence is composed of sandstone, shale, coal layers and limestone, all of which are overlain by Emeishan flood basalts. The basalts are in turn overlain by late Permian sandstone, siltstone and coal measures. Triassic strata consist of siltstone, sandstone, dolostone and limestone. More than 100 Pb–Zn deposits (occurrences) are hosted in Devonian to Permian carbonate rocks, but mostly in Carboniferous dolomitic limestone and dolostone (Fig. 1B and C). The NW-, EW- and NE-striking

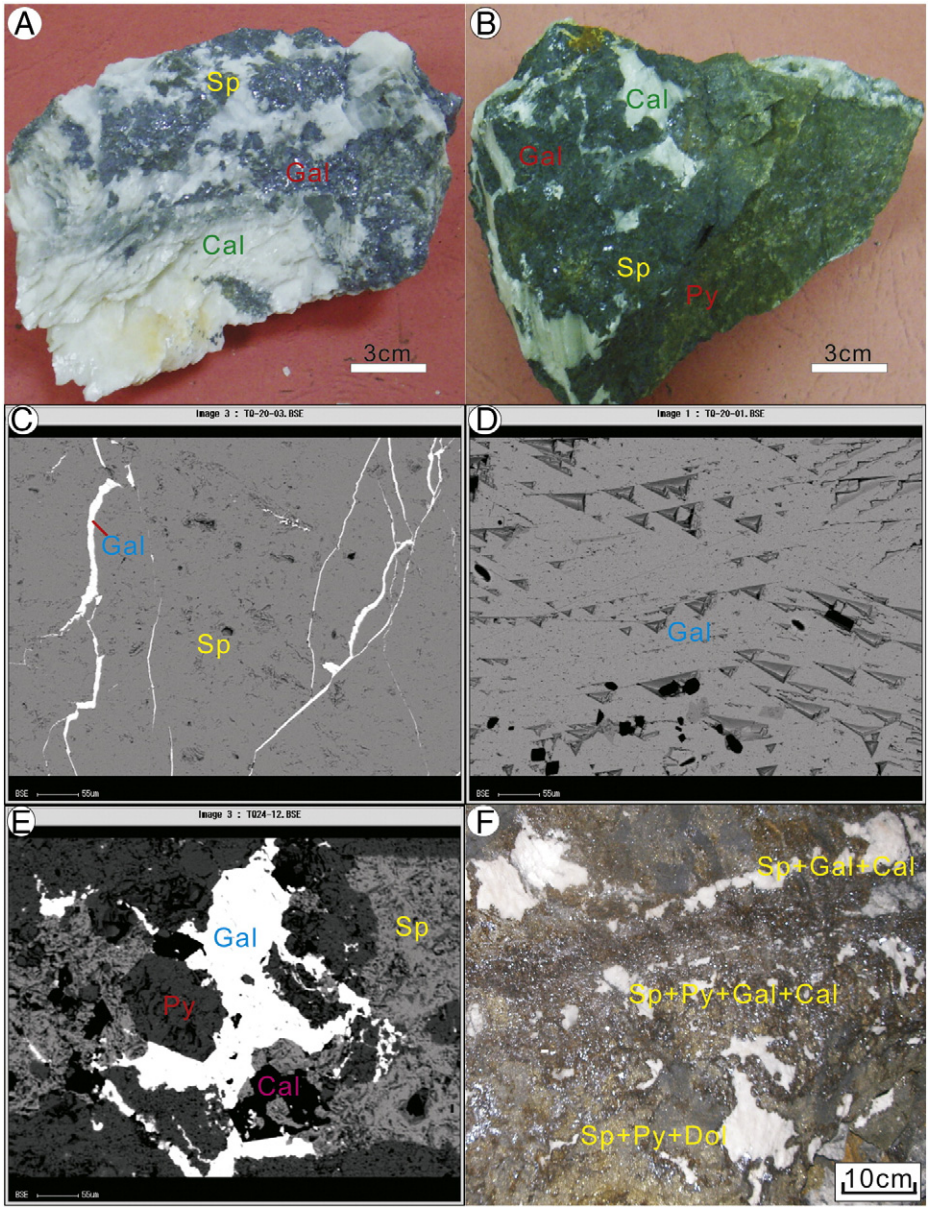

Fig. 4. Photographs and EPMA images of mineral assemblages in the Tianqiao Pb–Zn deposit. A: granular sphalerite (Sp)–massive galena (Gal)–lumpy calcite (Cal) assemblage; B: disseminated Sp–massive pyrite (Py)–vein Gal–patch Cal assemblage; C: vein Gal in the early stage Sp; D: Gal pressure shadows; E: metasomatic Sp–granular Py–patch Cal–vein Gal; F: From bottom to top of the No. 1 ore body, the mineral assemblage change from Sp + Py + Dolomite (Dol) through Sp + Py + Gal + Cal to Sp + Gal + Cal.

faults in this district control the distribution of the deposits (Fig. 1B; Zhou et al., 2013b). The Tianqiao deposit is located in the northwestern part of the NW-trending Yadu–Mangdong fault (Fig. 1B and C; Zhou et al., 2013a) and the new found Banbanqiao deposit is situated in the central part of the EW-trending Dushan–Huamiaozai fault (Fig. 1B and C).

3. Deposit geology

3.1. Tianqiao Pb–Zn deposit

The Tianqiao deposit is hosted in the Upper Devonian to Lower Carboniferous dolomitic limestone and dolomite (Figs. 1C and 2A; Zhou et al., 2013a). In the Tianqiao deposit, Devonian to Permian sedimentary rocks form the Tianqiao anticline, which is crosscut by NW-, NE- and EW-trending faults (Fig. 2A). The Tianqiao anticline has an axial plane that strikes N45–60°W and both of its limbs have roughly the same strike and dip to the NE and SW at angles of 30–45°. Being the largest fault in the mining district, F_{37} cuts across the Tianqiao anticline (Fig. 2A). This fault is 14 km long and is marked by a 1 to 6 m wide shear zone. It strikes 50–90°NE and dips 50–70°NE (Fig. 3A). Movement along the fault is oblique with 20 to 60 m of vertical displacement and 80 to 240 m of horizontal displacement.

Major ore bodies occur in dolomitic limestone and dolomite of the Lower Carboniferous strata, which form the NW-trending nose of the plunging anticline, and are located along the thrust fault F_{37} (Fig. 2A). Thirty-two ore bodies occur in two limbs of the Tianqiao anticline where they form two ore clusters near the axis in the northeastern and southern limbs (Fig. 2A). Underground mining and exploratory drill holes in these two clusters provide excellent access to the major No. 1 and No. 2 ore bodies (Fig. 3A), where the ore samples are collected. Another ore cluster occurs in the southwestern limb of the anticline, away from the axis. Ore bodies in this cluster are widely oxidized with no primary ores. These ore bodies have higher Zn than Pb with Zn/Pb ratios mostly between 2 and 8. Ores from these ore bodies also contain small amounts of Ge–Ga–Cd and Ag that are hosted in crystal lattice of sphalerite and galena, respectively and/or other possible mineral phases (i.e. greenockite, acanthite; Zhou et al., 2011). No. 1 ore body is the largest one, which is 200 m long, 100 m wide and 1.3 to 1.8 m thick and contains 1 Mt of ores at a grade of 1.3 to 10.5 wt.% Pb and 5.7 to 18.8 wt.% Zn. From the bottom of this ore body to its top, mineral assemblages show regular changes that range from sphalerite–pyrite–dolomite through sphalerite–pyrite–galena–calcite to sphalerite–galena–calcite assemblages (Fig. 4F).

Ores in this deposit have experienced hydrothermal and supergene oxidizing processes. The hydrothermal period is composed of two main stages: sulfide-carbonate and carbonate stages. In the sulfide-carbonate stage, three principal mineral assemblages formed (Zhou et al., 2013a). In the sphalerite–pyrite–dolomite assemblage, brownish sphalerite is fine- to coarse-grained (0.08 to 12 mm) with xenomorphic to automorphic granular textures (Fig. 4A, C and F). It occurs as massive and individual grains are commonly skeletal with a well-developed cleavage. Pyrite is coarse-grained (2–5 mm), has both octahedral and cubic forms and commonly occurs as disseminations in the wall rocks adjacent to the ores (Fig. 4F). Dolomite is lumpy and patchy, about 10 cm in width (Fig. 4F). In the sphalerite–pyrite–galena–calcite assemblage, brown–yellow sphalerite is fine- to coarse-grained (0.05 to 10 mm) with xenomorphic to automorphic granular textures. It occurs in disseminated aggregates (Fig. 4B, E and F). Associated pyrite is coarse-grained (2–5 mm), has both octahedral and cubic forms and commonly occurs as bands in the wall rocks adjacent to the ores. Galena has a granular and corrugated texture (Fig. 4A, D and E), and its individual grains are 0.1 to 15 mm in diameter, have a cubic cleavage and have obvious deformation. Calcite occurs patchy and about 6 cm in width (Fig. 4F). In the sphalerite–galena–calcite assemblage, light yellow sphalerite is fine grained (0.01 to 1 mm) with xenomorphic granular textures (Fig. 4F). It occurs in banded forms. Galena occurs as veins filling in the previous formed sphalerite (Fig. 4C). Calcite occurs in tiny veins (Fig. 4B and F). The carbonate stage mainly forms calcite that occurs in veins in dolostone and limestone. More details about mineral paragenesis of this deposit are described by Zhou et al. (2013a) and are listed in Table 1.

Wall rock alterations include dolomitization, calcitization, Fe–Mn carbonatization and ferritization. All are closely associated with Pb–Zn mineralization, but only Fe–Mn carbonatization and ferritization are good indicators for ore prospecting. Fe–Mn carbonatization results in the formation of Fe (Mn)-bearing light brown, maroon or puce dolostone, which surrounds Pb–Zn ore bodies (Zhou et al., 2013a). Ferritization occurs as Fe–capping of sulfide Pb–Zn ore bodies and its intensity is positively correlated with Pb–Zn mineralized scale.

3.2. Banbanqiao Pb–Zn deposit

The newly discovered Banbanqiao deposit is hosted by the Upper Carboniferous Huanglong-Maping Formation, which consists of limestone, dolomitic limestone and dolostone (Figs. 2B and 3B). The deposit is structurally controlled by the EW-trending Dushan–Huamiaozai fault and NW-trending F_1 fault, and the Ertaipo anticline (Figs. 1C, 2B and 3B). Ores in the Banbanqiao deposit are dominated by sulfide ores, with small amounts of oxidized ores near the surface. The mineralogy is relatively simple and includes sphalerite, pyrite, galena, calcite and dolomite (Fig. 5A). The deposit contains Pb–Zn ores about 1.5 Mt at grades of 0.26 to 10.3 wt.% Pb and 0.81 to 28.8 wt.% Zn with Zn/Pb ratios mostly between 4 and 12. Sulfides have high Cd and Ag contents. These metals mainly occur as solid solutions within sphalerite (1395 to 2906 ppm Cd) and galena (27 to 85 g/t Ag), respectively (Zhou et al., 2011).

Sulfide ores from this deposit have granular, metasomatic, filling, and crush textures and massive, disseminated, brecciated, veined and banded structures. In granular ores, pyrite is sub- to euhedral, and galena and sphalerite are subhedral and xenomorphic. In filling ores, fine-grained galena and pyrite which are xenomorphic and subhedral, together with xenomorphic calcite, fill the inter-granular space between sphalerite crystals. Broken pyrite grains are cemented by sphalerite,

Table 1
Mineral paragenesis of the Tianqiao and Banbanqiao deposits, SW China.

Tianqiao deposit					
Periods	Hydrothermal				Supergene oxidizing
Stages	Sulfide–carbonate			Carbonate	Oxidized
Mineral assemblage	Sp + Py + Dol	Sp + Py + Gal + Cal	Sp + Gal + Cal	Dol + Cal	Lim + Cer
Brown sphalerite	▬	—			
Brown yellow sphalerite	—	▬	—		
Light yellow sphalerite		—	▬		
Pyrite	▬	▬	—		
Galena		—	▬		
Dolomite	▬	▬	▬	▬	
Calcite	—	▬	▬	▬	
Limonite					▬
Cerusite					▬

Banbanqiao deposit					
Periods	Hydrothermal				Supergene oxidizing
Stages	Sulfide–carbonate			Carbonate	Oxidized
Mineral assemblage	Sp + Py + Cal	Sp + Py + Gal + Cal	Sp + Gal + Cal	Dol + Cal	Lim + Cer
Brown sphalerite	▬	—			
Red brown sphalerite	—	▬	—		
Light yellow sphalerite		—	▬		
Euhedral pyrite	▬	—			
Subhedral pyrite	—	▬	—		
Anhedral pyrite		—	▬		
Galena		—	▬		
Dolomite	▬	▬	▬	▬	
Calcite	—	▬	▬	▬	
Limonite					▬
Cerusite					▬

Sp, sphalerite; Py, pyrite; Gal, galena; Dol, dolomite; Cal, calcite; Lim, limonite; Cer, Cerusite — Less ▬ More.

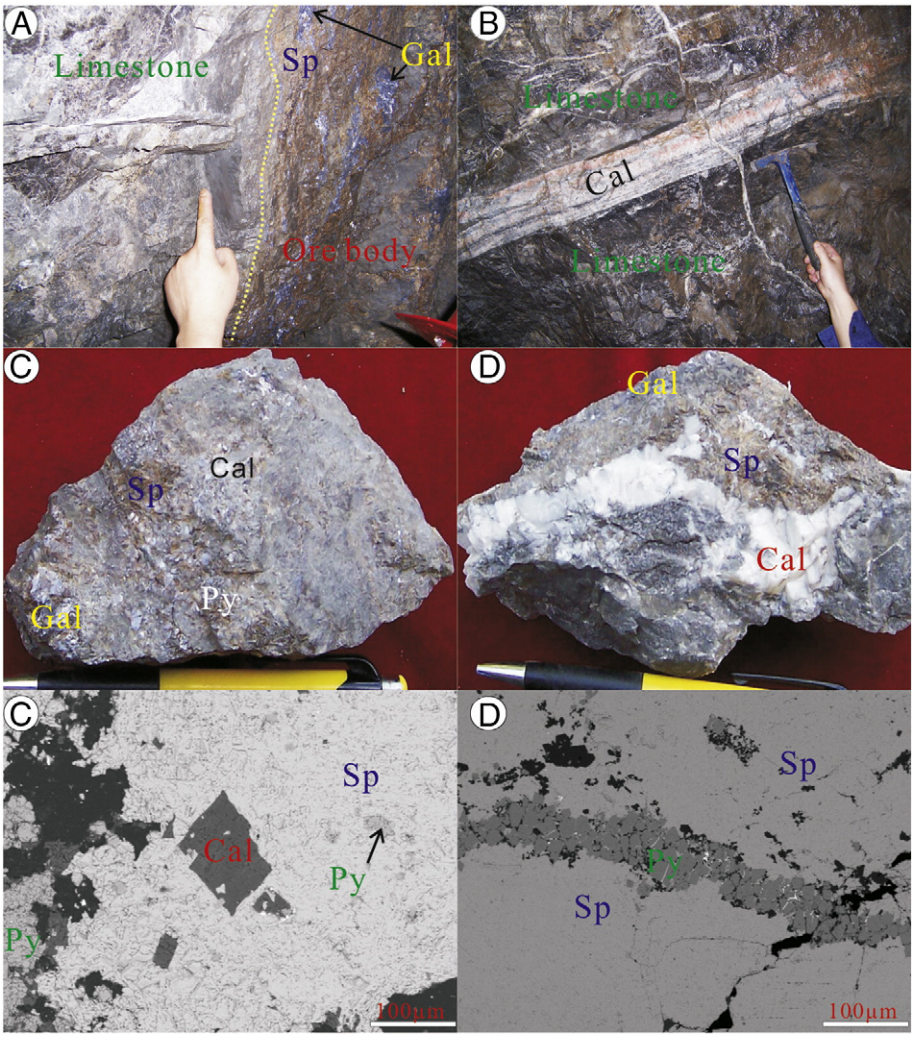

Fig. 5. Photographs and EPMA images of mineral assemblages and wall rocks of the Banbanqiao Pb–Zn deposit. A: boundary of ore body and host rocks, massive sphalerite (Sp) and vein galena (Gal); B: thick and thin veins calcite (Cal) in limestone; C: massive and vein Sp–granular pyrite (Py)–patch Cal assemblage; D: massive Sp-patchy and vein Cal-disseminated Gal assemblage; E: the early stage Py and Cal in the middle stage granular Sp; F: the late stage granular Py in the early stage Sp.

galena and clay minerals. In metasomatic ores, pyrite is partially replaced by sphalerite and galena, resulting in a skeletal and embayed texture. Replacement of sulfides by calcite occurs from the interior and forms skeletal texture. In this metasomatic ore type, string and sharply angular galena finally replaces sphalerite, pyrite and calcite.

Metallogenic processes of the Banbanqiao deposit also include hydrothermal and supergene oxidizing periods. The hydrothermal period can also be divided into sulfide-carbonate and carbonate stages (Fig. 5A and B). The sulfide-carbonate stage contains three mineral assemblages: sphalerite–galena–calcite, sphalerite–pyrite–calcite and sphalerite–pyrite–galena–calcite. Three stages of pyrite and sphalerite can be distinguished in these assemblages (Fig. 5A and C–F). Sphalerite of the early stage is brown, sub- to euhedral and 2–8 mm in size (Fig. 5A and C). Pyrite of this stage is euhedral coarse-grained with grain size between 2 and 5 mm (Fig. 5C and E). Sphalerite of the middle stage (Fig. 5D) is red brown and subhedral (0.5–5 mm) and pyrite (Fig. 5E) is medium to coarse-grained and sub- to euhedral (0.5–3 mm). Pyrite from the final stage is anhedral–subhedral, with a grain size less than 0.8 mm. Sphalerite (Fig. 5F) of this stage is light yellow, transparent to sub-transparent and has a variable grain size (0.05–0.8 mm). More details about mineral paragenesis are listed in Table 1. The wall rock alterations are similar to the Tianqiao deposit, including dolomitization, calcitization, Fe–Mn carbonatization and ferritization.

4. Sampling and analytical methods

4.1. Sample collection and preparation

Twenty-eight representative ores from drill cores and mining adits of the Tianqiao deposit and nine ores from drill cores of the Banbanqiao deposit have been sampled (Fig. 3A and B). Different stages of sphalerite from the same ores (Table 1) can be separated based on mineral paragenesis, textural and structural characteristics, and crosscutting relationships. Forty-nine sphalerite grains separated from these ore samples are handpicked under a binocular microscope. In addition, eleven bulk-rock samples of Sinian to Permian sedimentary rocks and Permian Emeishan flood basalts are collected from the Erdaogou profile in the central part of the Sichuan–Yunnan–Guizhou Pb–Zn metallogenic province (Han et al., 2007; Zhou et al., 2013a). Analytical details are listed in Table 2 and are shown in Fig. 3.

4.2. Zinc isotope analyses

Sphalerite and bulk-rock samples were digested in HCl and HNO_3 + HF, respectively and then taken up in 6N HCl + 0.001% H_2O_2. Zinc was separated from matrix elements using anion exchange chromatography (Tang et al., 2006), a modified procedure from

Table 2
Zn–S–Pb isotopic compositions of sphalerite, sedimentary rocks and basalts in the Tianqiao and Banbanqiao Pb–Zn deposits, SW China.

Nos.	Objects	Positions	Mcineral assemblages	Stages	$\delta^{66}Zn_{JMC}$[a]	SD	NA	$\delta^{34}S_{CDT}$[a]	SD	NA	$^{208}Pb/^{204}Pb$	$^{207}Pb/^{204}Pb$	$^{206}Pb/^{204}Pb$
TQ3	Brown Sp	No.2 ore body ZK503-1780 m	Sp + Py + Dol	Early stage	0.00	0.04	3	14.0	0.30	2			
TQ6	Brown Sp	No.2 ore body ZK503-1780 m	Sp + Py + Dol	Early stage	0.01	0.05	3	13.9	0.15	2			
TQ8-2	Brown Sp	No.2 ore body ZK505-1760 m	Sp + Py + Gal + Cal	Middle stage	0.32	0.05	3	12.5	0.11	2			
TQ10	Brown–Yellow Sp	No.2 ore body ZK505-1760 m	Sp + Gal + Cal	Final stage	0.53	0.03	2	13.7	0.14	2			
TQ13	Brown Sp	No.2 ore body ZK505-1760 m	Sp + Py + Gal + Cal	Middle stage	0.24	0.05	3	11.7	0.09	2			
TQ16-2	Brown Sp	Inner of No.1 ore body Tunnel-1775 m	Sp + Py + Gal + Cal	Early stage	0.25	0.03	3	13.7	0.13	2			
TQ16-1	Brown–Yellow Sp	Inner of No.1 ore body Tunnel-1775 m	Sp + Py + Gal + Cal	Middle stage	0.35	0.04	3	12.3	0.08	2			
TQ17-2	Brown Sp	Inner of No.1 ore body Tunnel-1775 m	Sp + Py + Gal + Cal	Final stage	0.43	0.04	3	11.8	0.11	2			
TQ17-1	Brown–Yellow Sp	Inner of No.1 ore body Tunnel-1775 m	Sp + Py + Gal + Cal	Middle stage	0.36	0.06	3	12.2	0.12	2			
TQ17-2p[b]	Brown Sp	Inner of No.1 ore body Tunnel-1775 m	Sp + Py + Gal + Cal	Final stage	0.47	0.05	3	11.9	0.10	2			
TQ18	Brown Sp	No.1 ore body Tunnel-1775 m	Sp + Py + Gal + Cal	Middle stage	0.24	0.04	4	13.1	0.18	2			
TQ19	Brown–Yellow Sp	No.1 ore body Tunnel-1775 m	Sp + Gal + Cal	Final stage	0.58	0.04	3	13.9	0.12	3			
TQ20-1	Brown Sp	Outer of No.1 ore body Tunnel-1775 m	Sp + Gal + Cal	Early stage	0.11	0.05	3	12.0	0.09	2			
TQ20-2	Brown–Yellow Sp	Outer of No.1 ore body Tunnel-1775 m	Sp + Gal + Cal	Middle stage	0.44	0.07	3	11.7	0.06	2			
TQ24-1	Brown Sp	Outer of No.1 ore body Tunnel-1775 m	Sp + Gal + Cal	Early stage	0.39	0.04	3	12.3	0.07	2	38.930	15.724	18.517
TQ24-2	Brown–Yellow Sp	Outer of No.1 ore body Tunnel-1775 m	Sp + Gal + Cal	Middle stage	0.48	0.03	4	11.9	0.12	2	38.929	15.725	18.527
TQ24-3	Light Yellow Sp	Outer of No.1 ore body Tunnel-1775 m	Sp + Gal + Cal	Final stage	0.57	0.03	3	10.9	0.07	2	38.875	15.708	18.481
TQ25	Brown–Yellow Sp	No.1 ore body ZK501-1780 m	Sp + Py + Dol	Early stage	0.12	0.04	2	12.1	0.06	2	38.888	15.713	18.490
TQ26	Brown–Yellow Sp	No.1 ore body ZK501-1780 m	Sp + Py + Gal + Cal	Middle stage	0.32	0.05	3	12.2	0.09	2			
TQ53-1	Brown Sp	Inner of No.1 ore body Tunnel-1775 m	Sp + Py + Gal + Cal	Early stage	0.05	0.04	3	13.8	0.12	2			
TQ53-2	Brown–Yellow Sp	Inner of No.1 ore body Tunnel-1775 m	Sp + Py + Gal + Cal	Middle stage	0.18	0.05	3	13.6	0.15	2			
TQ54-1	Brown–Yellow Sp	Outer of No.1 ore body Tunnel-1775 m	Sp + Gal + Cal	Middle stage	0.49	0.04	3	12.2	0.08	2			
TQ54-2	Brown Sp	Outer of No.1 ore body Tunnel-1775 m	Sp + Gal + Cal	Early stage	0.22	0.03	2	12.0	0.10	3	38.888	15.714	18.504
TQ55	Brown Sp	No.1 ore body ZK501-1780 m	Sp + Py + Gal + Cal	Middle stage	0.29	0.03	4	12.6	0.12	2			
TQ56-1	Brown–Yellow Sp	No.1 ore body ZK501-1780 m	Sp + Py + Dol	Early stage	0.09	0.04	3	12.2	0.10	2			
TQ56-2	Brown Sp	No.1 ore body ZK501-1780 m	Sp + Gal + Cal	Final stage	0.41	0.04	3	11.5	0.11	2			
TQ58	Brown Sp	No.1 ore body ZK501-1780 m	Sp + Py + Dol	Early stage	−0.01	0.03	3	13.9	0.12	2			
TQ60-2	Brown Sp	Inner of No.1 ore body Tunnel-1775 m	Sp + Py + Gal + Cal	Early stage	0.33	0.03	3	12.4	0.07	2			
TQ60-1	Brown–Yellow Sp	Inner of No.1 ore body Tunnel-1775 m	Sp + Py + Gal + Cal	Middle stage	0.19	0.04	2	12.3	0.08	2			
TQ62	Brown–Yellow Sp	No.1 ore body ZK502-1770 m	Sp + Py + Gal + Cal	Middle stage	0.30	0.05	3	12.4	0.06	2			
TQ62p[b]	Brown–Yellow Sp	No.1 ore body ZK502-1770 m	Sp + Py + Gal + Cal	Middle stage	0.31	0.04	2	12.3	0.05	2			
TQ64	Brown–Yellow Sp	No.1 ore body ZK502-1770 m	Sp + Py + Gal + Cal	Early stage	0.25	0.06	4	12.1	0.09	2			
TQ110	Brown Sp	No.1 ore body ZK502-1770 m	Sp + Gal + Cal	Final stage	0.56	0.05	3	11.2	0.09	2			
TQ105	Brown Sp	No.1 ore body ZK502-1770 m	Sp + Py + Dol	Early stage	0.06	0.05	3	12.3	0.11	3			
TQ081	Brown Sp	No.1 ore body ZK501-1760 m	Sp + Py + Dol	Early stage	−0.26	0.04	3	14.8	0.21	3			
TQ083	Brown Sp	No.1 ore body ZK501-1760 m	Sp + Py + Dol	Early stage	0.03	0.06	3	12.5	0.08	2			
TQ084	Brown–Yellow Sp	No.1 ore body ZK501-1760 m	Sp + Py + Dol	Early stage	0.04	0.05	3	12.6	0.07	2			
TQ085-1	Brown Sp	Inner of No.1 ore body Tunnel-1775 m	Sp + Py + Gal + Cal	Early stage	−0.01	0.07	3	12.5	0.06	2			
TQ085-2	Brown–Yellow Sp	Inner of No.1 ore body Tunnel-1775 m	Sp + Py + Gal + Cal	Middle stage	0.25	0.04	2	12.4	0.07	2			
TQ086	Brown Sp	No.2 ore body ZK505-1760 m	Sp + Py + Gal + Cal	Middle stage	0.36	0.05	4	12.3	0.10	2			
B04	Light Yellow Sp	Main ore body ZK-1-1752 m	Sp + Gal + Cal	Final stage	0.71	0.06	4	6.0	0.02	2	38.145	15.651	18.130
B08	Light Yellow Sp	Main ore body ZK-1-1750.5 m	Sp + Gal + Cal	Final stage	0.62	0.05	3	8.4	0.03	2	38.261	15.665	18.200

Table 2 (*continued*)

Nos.	Objects	Positions	Mcineral assemblages	Stages	$\delta^{66}Zn_{JMC}$[a]	SD	NA	$\delta^{34}S_{CDT}$[a]	SD	NA	$^{208}Pb/^{204}Pb$	$^{207}Pb/^{204}Pb$	$^{206}Pb/^{204}Pb$
B09	Brown Sp	Main ore body ZK-1-1748.5 m	Sp + Py + Cal	Early stage	0.25	0.05	3	6.4	0.01	2	38.229	15.674	18.153
B15	Red Brown Sp	Main ore body ZK-1-1749 m	Sp + Py + Gal + Cal	Middle stage	0.47	0.05	3	3.9	0.07	2	38.161	15.658	18.133
B17	Light Yellow Sp	Main ore body ZK-1-1750 m	Sp + Gal + Cal	Final stage	0.58	0.06	3	6.1	0.06	2	38.393	15.676	18.270
B18	Brown Sp	Main ore body ZK-2-1748.5 m	Sp + Py + Cal	Early stage	0.23	0.04	3	6.6	0.12	2	38.201	15.668	18.176
B20	Light Yellow Sp	Main ore body ZK-2-1750 m	Sp + Gal + Cal	Final stage	0.50	0.07	3	4.8	0.03	2	38.850	15.715	18.726
B21	Red Brown Sp	Main ore body ZK-2-1749 m	Sp + Py + Gal + Cal	Middle stage	0.36	0.05	3	9.0	0.11	2	38.154	15.656	18.029
B924	Brown Sp	Main ore body ZK-2-1748 m	Sp + Py + Cal	Early stage	0.07	0.05	2	7.1	0.06	3	38.286	15.701	18.159
D09-1	Dolostone	Sinian Dengying Fm.[c]	Pre-mineralization		−0.24	0.06	4						
D09-3	Sedimentary rocks	Middle Devonian Haikou Fm.[c]	Pre-mineralization		−0.19	0.06	3						
D09-5	Sedimentary rocks	Middle Devonian Haikou Fm.[c]	Pre-mineralization		0.06	0.06	2						
D09-7	Limestone	Upper Devonian Zaige Fm.[c]	Pre-mineralization		−0.22	0.05	3						
D22	Limestone	Lower Carboniferous Dapu Fm.[c]	Pre-mineralization		−0.12	0.04	3						
D23	Dolostone	Lower Carboniferous Baizuo Fm.[c]	Pre-mineralization		0.15	0.04	3						
D24	Dolostone	Lower Carboniferous Baizuo Fm.[c]	Pre-mineralization		0.17	0.05	3						
D09-10	Sedimentary rocks	Lower Permian Liangshan Fm.[c]	Pre-mineralization		−0.16	0.06	3						
Ems09-14	Basalts	Permian Emeishan Fm.[c]	Pre-mineralization		0.32	0.06	3						
Ems09-15	Basalts	Permian Emeishan Fm.[c]	Pre-mineralization		0.30	0.04	3						
Ems09-16	Basalts	Permian Emeishan Fm.[c]	Pre-mineralization		0.44	0.10	3						

Sp, sphalerite; Py, pyrite; Gal, galena; Dol, dolomite; Cal, calcite; Fm., formation; SD, standard deviation; NA, number of analyses.
Samples TQ16-1 and TQ16-2 are from the same hand specimen TQ16; Similarly, TQ17-1 and TQ17-2 from TQ17; TQ20-1 and TQ20-2 from TQ20; TQ24-1, TQ24-2 and TQ24-3 from TQ24; TQ53-1 and TQ53-2 from TQ53; TQ54-1 and TQ54-2 from TQ54; TQ56-1 and TQ56-2 from TQ56; TQ085-1 and TQ085-2 from TQ085. Different stages of sphalerite from the same ores can be separated by textural and structural observations (Figs. 4 and 5 and Table 1).

[a] Mean over n number of repeats.

[b] Samples are used for procedural repeats.

[c] Sinian to Permian sedimentary rocks and Permian Emeishan flood basalts were collected from the Erdaogou profile in the central part of the Sichuan–Yunnan–Guizhou Pb–Zn metallogenic province (Han et al., 2007; Zhou et al., 2013a).

described by Maréchal et al. (1999). H_2O used in the experiment was purified using the Milli-Q system, with electric resistance of 18.2 MΩ. HCl, HNO_3 and HF were purified by sub-boiling distillation and the purifications of all reagents were accomplished in an ultra-clean laboratory. Zinc isotope analyses were carried out using Nu Plasma HR MC-ICP-MS at the Key Laboratory of Isotope Geology, Department of Land and Resources, Institute of Geology, Chinese Academy of Geological Sciences (Li et al., 2008). Mass discrimination effects were corrected

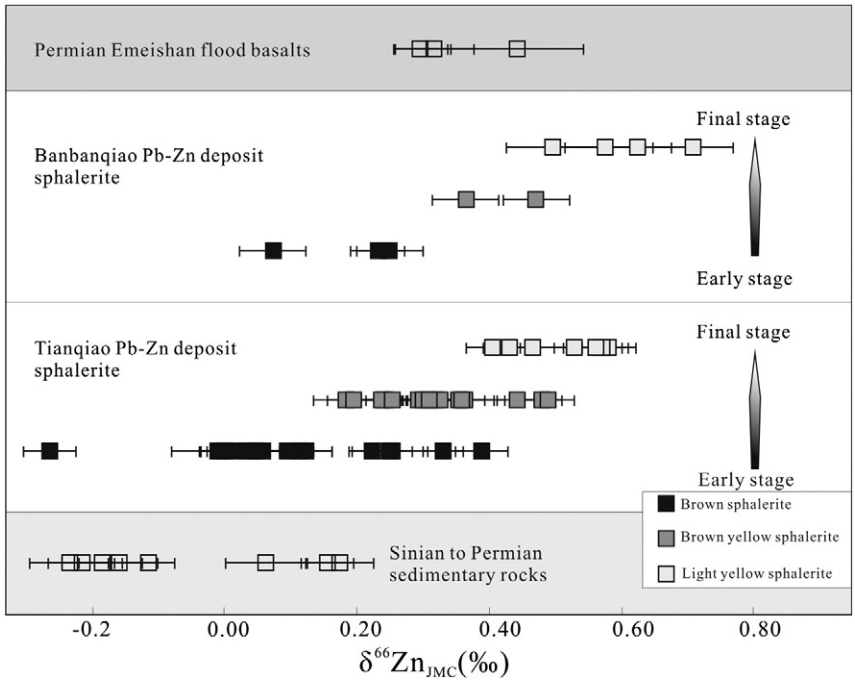

Fig. 6. Zinc isotopic compositions of sphalerite from the Tianqiao and Banbanqiao Pb–Zn deposits, and the potential zinc source rocks (Sinian to Permian sedimentary rocks and Permian Emeishan flood basalts). It is clear that the late staged sphalerite enriches in heavy Zn isotope and the majority of the hydrothermal sphalerite has heavier zinc isotope than the county rocks.

using a combined sample-standard bracketing and inter-element correction procedure (Li et al., 2008; Mason et al., 2004a, 2004b). Accuracy and reproducibility were assessed by replicate analyses of the international standards BCR-2 (basalt), which yielded an average $\delta^{66}Zn$ value of 0.28 ± 0.09 (2σ, n = 6), within error in agreement with the previously published values by Mason et al. (2004a, 2004b, 2005) and Kelley et al. (2009). Samples TQ17-2 and TQ62 are used for procedural repeats. These repeated analyses demonstrate that the duplications are well within the errors. Each result is the mean value over N number of repeats, and all results are reported relative to the Lyon JMC 3-0749L zinc standard (Maréchal et al., 1999).

4.3. Sulfur and lead isotope analyses

Sulfur isotope analyses are carried out at the State Key Laboratory of Environmental Geochemistry, Institute of Geochemistry, Chinese Academy of Sciences, using a Continuous Flow Mass Spectrometer. GBW 04415 and GBW 04414 Ag_2S are used as the external standards, and the relative errors (2σ) are better than 0.1‰ from the replication of standard materials. Sulfur isotopic compositions are reported relative to the Canyon Diablo Troilite (CDT).

Lead isotope analyses are carried out using the GV Isoprobe-T Thermal Ionization Mass Spectrometer at the Beijing Institute of Uranium Geology. The analytical procedure involves dissolution of samples using HF and $HClO_4$ in crucibles, followed by addition of an anion exchange resin to purify Pb. Analytical results for the standard NBS 981 are $^{208}Pb/^{204}Pb$ = 36.611 ± 0.004 (2σ), $^{207}Pb/^{204}Pb$ = 15.457 ± 0.002 (2σ) and $^{206}Pb/^{204}Pb$ = 16.937 ± 0.002 (2σ), in agreement with the reference values (Belshaw et al., 1998).

5. Analytical results

5.1. Zn isotopic compositions

Sphalerite from the Tianqiao deposit has $\delta^{66}Zn$ values ranging from −0.26 to +0.58‰, with a mean value of +0.26‰ (Table 2). Sphalerite, which precipitated in the early, middle and final mineralization stage of the Tianqiao deposit, has $\delta^{66}Zn$ values range from −0.26 to +0.39‰, +0.18 to +0.49‰ and +0.41 to +0.58‰, respectively (Table 2). Sphalerite from the Banbanqiao deposit has narrow $\delta^{66}Zn$ values range of +0.07 to +0.71‰, with a mean value of +0.42‰ (Table 2). The zinc isotopic compositions of sphalerite from the three stages of the Banbanqiao deposit range from +0.07 to +0.25‰, +0.36 to +0.47‰ and +0.50 to +0.71‰, respectively (Table 2). So, in both deposits late-stage sphalerite is enriched in heavy zinc isotope (Fig. 6). In addition, sphalerite in the center (near to bottom) part of the No. 1 ore body of the Tianqiao deposit (Fig. 7) has relatively lower $\delta^{66}Zn$ values (−0.01 to +0.43‰) than those (+0.11 to +0.57‰) in the periphery (near to top).

Zinc isotopic compositions of Sinian to Permian sedimentary bulk-rock samples range from −0.24 to +0.22‰, with a mean value of −0.07‰ (Table 2). Permian Emeishan flood basalts samples have whole-rock $\delta^{66}Zn$ values of +0.30 to +0.44‰, with a mean value of +0.35‰ (Table 2). Although part of sphalerite lie within the range of

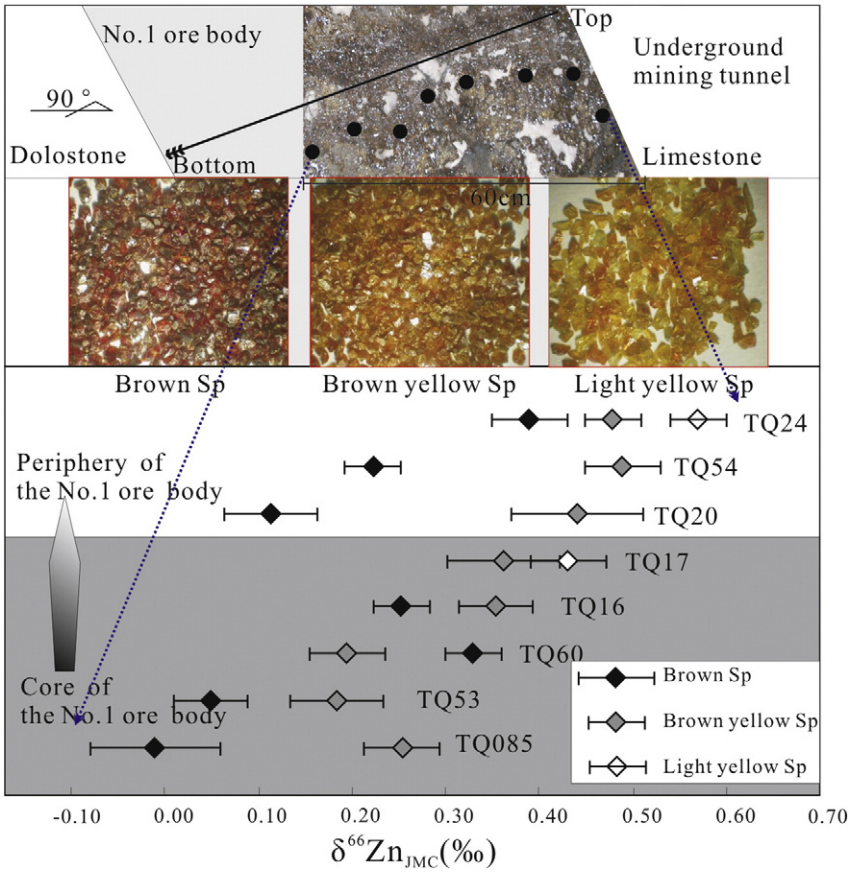

Fig. 7. $\delta^{66}Zn$ values of sphalerite from the center towards top of the No. 1 ore body in the Tianqiao deposit. It shows that the $\delta^{66}Zn$ values increase gradually from the center (near to bottom of the ore body) to periphery (near to top of the ore body) and the late staged light yellow sphalerite enriches in heavy zinc isotope.

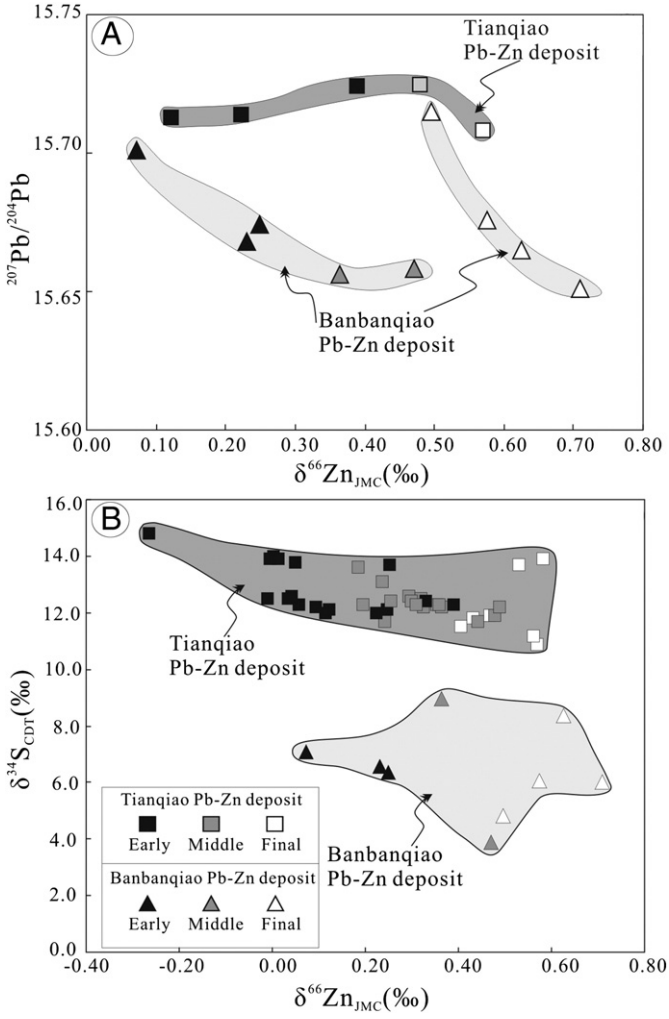

Fig. 8. Plot of $\delta^{66}Zn$ values vs. $^{207}Pb/^{204}Pb$ ratios shows one group for sphalerite from the Tianqiao Pb–Zn deposit, whereas two groups for sphalerite from the Banbanqiao Pb–Zn deposit (A); and plot of $\delta^{66}Zn$ vs. $\delta^{34}S$ values shows a weakly negative correlation for sphalerite from the Tianqiao Pb–Zn deposit, whereas no correlation for sphalerite from the Banbanqiao Pb–Zn deposit (B).

sedimentary and volcanic rocks, the majority of sphalerite has heavier zinc isotope than the country rocks (Fig. 6).

5.2. S–Pb isotopic compositions

Sphalerite from the Tianqiao deposit has $\delta^{34}S_{CDT}$ values ranging from +10.9 to +14.8‰, which are significantly higher than those of sphalerite (+3.9 to +9.0‰) from the Banbanqiao deposit (Fig. 8 and Table 2). Sphalerite from the Tianqiao deposit has $^{206}Pb/^{204}Pb$ range from 18.481 to 18.527, $^{207}Pb/^{204}Pb$ range from 15.708 to 15.725 and $^{208}Pb/^{204}Pb$ range from 38.875 to 38.930 (Table 2), whereas sphalerite from the Banbanqiao deposit has $^{206}Pb/^{204}Pb$ ratios between 18.029 and 18.726, $^{207}Pb/^{204}Pb$ ratios between 15.651 and 15.715 and $^{208}Pb/^{204}Pb$ ratios between 38.145 and 38.450 (Table 2). Lead isotope of sphalerite from the Tianqiao deposit is more radiogenic than those from the Banbanqiao deposit (Fig. 9).

6. Discussion

6.1. Possible causes of Zn isotope variations

Previous studies of Zn isotopes in hydrothermal systems indicated that ^{64}Zn-enriched sulfides occurred in early parts of the hydrothermal systems, whereas the residual fluids and late precipitates have higher $\delta^{66}Zn$ values (Archer et al., 2004;Gagnevin et al., 2012; John et al., 2008; Kelley et al., 2009; Mason et al., 2005; Wilkinson et al., 2005). Several causes are proposed to explain the evolution from light to heavy zinc isotope, including temperature gradient (Mason et al., 2005; Toutain et al., 2008), mixing of multiple zinc sources (Wilkinson et al., 2005) and kinetic Raleigh fractionation (Gagnevin et al., 2012; Kelley et al., 2009).

Studies on fumarolic gases and their condensates reveal large variations of $\delta^{66}Zn$ values ranging from +0.05 to +0.85‰ and from +1.48 to +1.68‰, respectively. These variations were thought to be due to temperature (297 to 590 °C) dependent zinc isotope fractionation (Toutain et al., 2008). However, Maréchal and Sheppard (2002) demonstrated experimentally that temperature variations of 30 to 50 °C have no effect on Zn isotopic compositions. Wilkinson et al. (2005) also suggested that there exists no correlation between $\delta^{66}Zn$ values and temperature differences from 60 to 250 °C. The homogenization temperatures of fluid inclusions in calcite and sphalerite from the Tianqiao (150 to 260 °C) and Banbanqiao (120 to 240 °C) deposits are similar

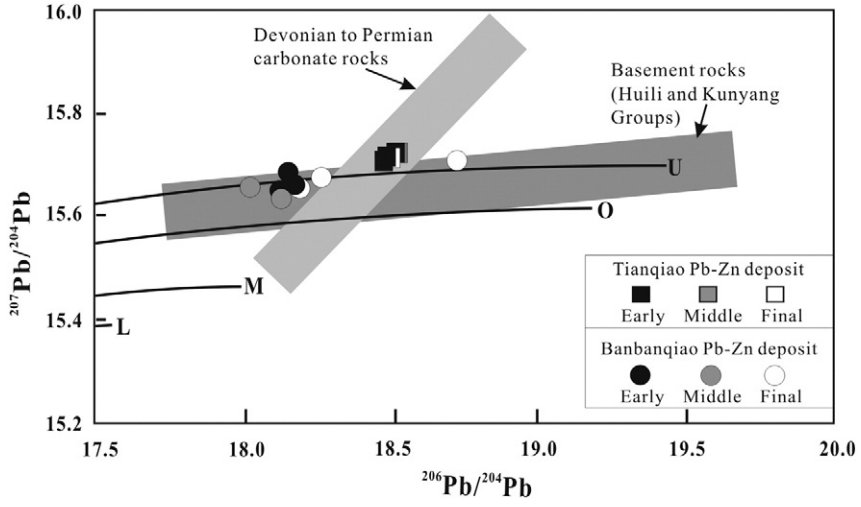

Fig. 9. Plot of $^{207}Pb/^{204}Pb$ vs. $^{206}Pb/^{204}Pb$ ratios of sphalerite from the Tianqiao and Banbanqiao Pb–Zn deposits. Trends for the upper crust (U), orogenic belt (O), mantle (M) and lower crust (L) are taken from Zartman and Doe (1981). Pb isotope data of Devonian to Permian carbonate rocks and Precambrian basement rocks are taken from Zheng and Wang (1991), Zhou et al. (2001, 2013a, 2013b, 2013c), Huang et al. (2004), Han et al. (2007) and Li et al. (2007a).

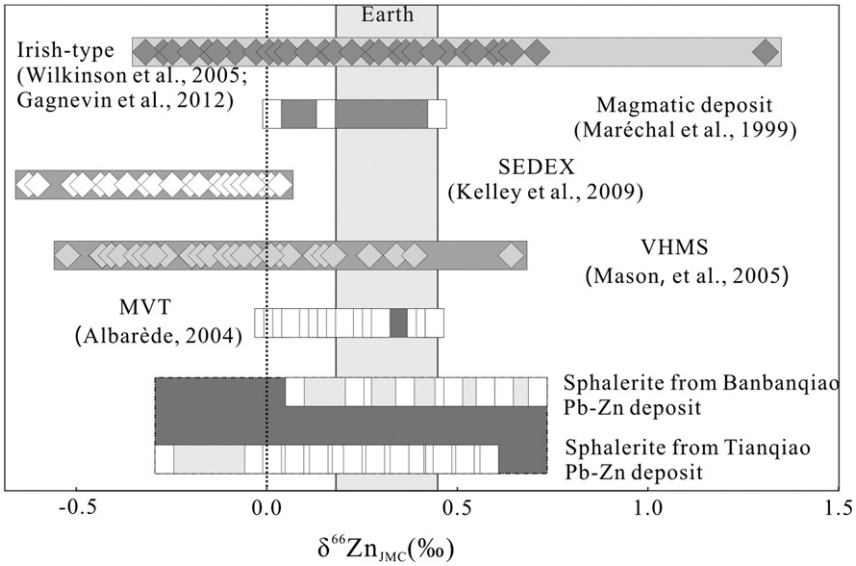

Fig. 10. Zinc isotopic compositions of sphalerite from the Tianqiao and Banbanqiao Pb–Zn deposits are compared with those from different ore genesis deposits. Zinc isotope data of sphalerite from the magmatic-type deposits are taken from Maréchal et al. (1999), those from the MVT-type deposits are taken from Albarède (2004), those from the Irish-type deposits are taken from Wilkinson et al. (2005) and Gagnevin et al. (2012), those from the VHMS-type deposits are taken from Mason et al. (2005) and those from the SEDEX-type deposits are taken from Kelley et al. (2009).

and indicate that both deposits belong to low temperature hydrothermal deposits (Han et al., 2004, 2007; Zhou et al., 2011, 2013a), so we consider that temperature gradient should not be the key cause for the observed Zn isotopes variations.

In the western Yangtze Block, southwest China, the basements are the Dongchuan, Kunyang and Huili Groups that consist of greywackes, but their zinc isotopic compositions are not available. The mean δ^{66}Zn value (+0.08‰) of greywackes in the Irish-type Pb–Zn deposits (Wilkinson et al., 2005) is used as a possible reference value for that of the basements in the metallogenic province. The younger cover sequences, Sinian to Permian sedimentary rocks and Permian Emeishan flood basalts, potential zinc source rocks have δ^{66}Zn values within the range of sphalerite from both deposits (Fig. 6), precluding the mixing of multiple zinc sources as the key factor controlling spatial and temporal variations of zinc isotopes.

Rayleigh fractionation of zinc isotope increases δ^{66}Zn values from the early to late stage (Gagnevin et al., 2012; Kelley et al., 2009; Mason et al., 2005; Wilkinson et al., 2005). Sphalerites from both deposits show such a trend in zinc isotope evolution (Figs. 6 and 7), indicating that Rayleigh fractionation could have occurred. This process has been used to explain the variations of zinc isotope in several deposits such as the Alexandrinka (VHMS-type; Mason et al., 2005), Irish Midlands (Irish-type; Wilkinson et al., 2005), Red Dog (SEDEX-type; Kelley et al., 2009) and Navan (Irish-type; Gagnevin et al., 2012). Thus, Rayleigh fractionation is likely the dominant factor controlling the observed temporal and spatial (Figs. 6 and 7) variations of zinc isotope in the two studied deposits.

6.2. Possible sources of sulfur and metals in the hydrothermal system

Sulfide ores from the Tianqiao and Banbanqiao Pb–Zn deposit have simple sulfide assemblages of galena, sphalerite and pyrite, and lack sulfates (Zhou et al., 2011, 2013a). Sulfur isotopic compositions of sulfides approximately represent the δ^{34}S values of the hydrothermal fluids (e.g., Basuki et al., 2008; Dixon and Davidson, 1996; Ohmoto et al., 1990; Seal, 2006). Sphalerite from both deposits has $\delta^{34}S_{CDT}$ values ranging from +3.9 to +14.8‰ (Table 2), unlike mantle-derived magmatic sulfur (~0‰; Chaussidon et al., 1989). Gypsum and barite from evaporates in the hosting Devonian to Permian strata have $\delta^{34}S_{CDT}$ values of ~+15‰ and +22 to +28‰, respectively (Han et al., 2007; Liu and Lin, 1999; Zhou et al., 2013a), similar to Cambrian to Permian seawater sulfates (+15 to +35‰; Claypool et al., 1980). Thermal chemical reduction of sulfate to sulfide can lower δ^{34}S values up to +15‰ in the MVT-type hydrothermal systems (e.g., Machel et al., 1995; Ohmoto and Goldhaber, 1997; Ohmoto et al., 1990) such that the reduced sulfur in ores may have been derived from evaporates in the host strata by thermal chemical sulfate reduction. The total range of homogenization temperatures of the fluid inclusions between 120 and 260 °C (Zhou et al., 2013a) exclude bacterial sulfate reduction, which could result in a larger sulfur isotope fractionation (in an open system). In addition, all sphalerites from the Tianqiao deposit have δ^{34}S values (+10.9 to +14.8‰) higher than those of the Banbanqiao (+3.9 to +9.0‰) deposit (Fig. 8 and Table 2) which may be due to evaporates having variable δ^{34}S values in different ages of the host rocks (Claypool et al., 1980), i.e. Upper Devonian to Lower Carboniferous versus Upper Carboniferous, respectively.

U and Th contents of sphalerite are too low to influence their Pb isotopic compositions, whereas Pb isotopic compositions of contrasted wall rocks of Devonian to Permian carbonates and Precambrian basements need to be corrected with ages (e.g., Carr et al., 1995; Muchez et al., 2005). Studies in the Sichuan–Yunnan–Guizhou Pb–Zn metallogenic province have reported hydrothermal calcite Sm–Nd ages of the Huize and Maozu Pb–Zn deposits at 222 ± 14 Ma (Li et al., 2007b) and 196 ± 13 Ma (Zhou et al., 2013c), respectively, and sulfide Rb–Sr ages of the Paoma and Tianqiao Pb–Zn deposits at 200.1 ± 4.0 Ma (Lin et al., 2010) and 191.9 ± 6.9 Ma (Zhou et al., 2013a), respectively. Thus, ~200 Ma was used to correct the Pb isotope. In the plot of $^{207}Pb/^{204}Pb$ vs. $^{206}Pb/^{204}Pb$ (Fig. 9), all samples plot close to the upper crustal lead evolution curve (Zartman and Doe, 1981). Moreover, samples from the Tianqiao deposit plot in the field of the age-corrected Devonian to Permian carbonates, whereas those from the Banbanqiao deposit plot in the age-corrected basement field (Fig. 9). This suggests that at least lead in the Tianqiao and Banbanqiao deposits was mainly originated from the carbonate host rocks and the basements, respectively.

6.3. Implications of Zn, S and Pb isotopes

The nearly linear correlation between Zn and Pb isotopic compositions of sphalerite from the Tianqiao deposit (Fig. 8A) indicates that

Pb–Zn metals may be originated from the same source rocks, i.e. the Paleozoic carbonate host rocks as suggested by Pb isotope. Because of the same sources of Zn–Pb metals and sulfur in the Tianqiao deposit and ^{34}S is heavier than ^{32}S resulting in ^{34}S-enriched in the early precipitated sphalerite (at the bottom of the hydrothermal system), so there is a weakly negative correlation between Zn and S isotopic compositions (Fig. 8B). Similarly, as the Zn–Pb metals and sulfur in the Banbanqiao deposit are sourced from the Paleozoic carbonate host rocks and the underlying Precambrian basements, respectively, so there is no obvious correlation between $\delta^{66}Zn$ and $\delta^{34}S$ values (Fig. 8B) could be explained by mixing of metal- and sulfur-bearing fluids (e.g., Kelley et al., 2009; Wilkinson et al., 2005).

Previous Zn isotope studies are available for the Cévennes MVT-type deposits (−0.06 to +0.42‰; Albarède, 2004), Irish-type deposits (Irish Midlands: −0.18 to +0.64‰, with one value at +1.33‰; Wilkinson et al., 2005 and Navan: −0.32 to +0.23‰; Gagnevin et al., 2012), Alexandrinka VHMS-type deposits (−0.03 to 0.23‰; Mason et al., 2005) and Red Dog SEDEX-type deposits (0 to +0.60‰; Kelley et al., 2009). Both the Tianqiao and Banbanqiao Pb–Zn deposits have unique zinc isotopic compositions (Fig. 10), suggesting that the Pb–Zn deposits in the Sichuan–Yunnan–Guizhou Pb–Zn metallogenic province differ from the type of magmatic hydrothermal, VHMS, SEDEX and typical MVT deposits, as demonstrated by geological and other geochemical evidences (e.g., Han et al., 2007; Zhou et al., 2013a).

7. Conclusions

(1) An increase in the $\delta^{66}Zn$ values of sphalerite from early to late stages in the ores from the Tianqiao and Banbanqiao deposits is observed and can be explained by kinetic Raleigh fractionation.
(2) Pb–Zn metals of the Tianqiao and Banbanqiao deposits were mainly originated from the Paleozoic carbonate host rocks and the Precambrian basements, respectively. Sulfur in the hydrothermal fluids of both deposits was derived from evaporates in the Paleozoic carbonate host rocks.

Acknowledgments

This research was financially supported by the National Basic Research Program of China (973 Program) (No. 2014CB440905) and National Natural Science Foundation of China (Nos. 41102055 and 41272111). Thanks are given to Prof. Ryan Mathur, Han-Jie Wen and Dr. Jian-Feng Gao, Xiao-Chun Li, Suo-Han Tang and Shi-Zhen Li for useful discussion. Comments and suggestions from Prof. Franco Pirajno, Khin Zaw and anonymous reviewers greatly improved the quality of the paper.

References

Albarède, F., 2004. The stable isotope geochemistry of copper and zinc. Rev. Mineral. Geochem. 55, 409–427.
Archer, C., Vance, D., Butler, I., 2004. Abiotic Zn isotope fractionations associated with ZnS precipitation. Geochim. Cosmochim. Acta 68, A325.
Basuki, N.I., Taylor, B.E., Spooner, E.T.C., 2008. Sulfur isotope evidence for thermochemical reduction of dissolved sulfate in Mississippi valley type zinc–lead mineralization, Bongara area, northern Peru. Econ. Geol. 103, 183–799.
Belshaw, N.S., Freedman, P.A., O'Nions, R.K., Frank, M., Guo, Y., 1998. A new variable dispersion double-focusing plasma mass spectrometer with performance illustrated for Pb isotopes. Int. J. Mass Spectrom. 181, 51–58.
Carr, G.R., Dean, J.A., Suppel, D.W., Heithersay, P.S., 1995. Precise lead isotope fingerprinting of hydrothermal activity associated with Ordovician to Carboniferous metallogenic events in the Lachlan fold belt of New South Wales. Econ. Geol. 90, 1467–1505.
Chaussidon, M., Albarède, F., Sheppard, S.M.F., 1989. Sulphur isotope variations in the mantle from ion microprobe analyses of micro-sulphide inclusions. Earth Planet. Sci. Lett. 92, 144–156.
Chung, S.L., Jahn, B.M., 1995. Plume–lithosphere interaction in generation of the Emeishan flood basalts at the Permian–Triassic boundary. Geology 23, 889–892.
Claypool, G.E., Holser, W.T., Kaplan, I.R., Sakai, H., Zak, I., 1980. The age curves of sulfur and oxygen isotopes in marine sulfate and their mutual interpretation. Chem. Geol. 28, 199–260.
Deng, H.L., Li, C.Y., Tu, G.Z., Zhou, Y.M., Wang, C.W., 2000. Strontium isotope geochemistry of the Lemachang independent silver ore deposit, northeastern Yunnan, China. Sci. China Ser. D Earth Sci. 43, 337–346.
Dixon, G., Davidson, G.J., 1996. Stable isotope evidence for thermochemical sulfate reduction in the Dugald River (Australia) strata-bound shale-hosted zinc–lead deposit. Chem. Geol. 129, 227–246.
Fernandez, A., Borrok, D.M., 2009. Fractionation of Cu, Fe, and Zn isotopes during the oxidative weathering of sulfide–rick rocks. Chem. Geol. 264, 1–12.
Fujii, T., Moynier, F., Pons, M.L., Albarède, F., 2011. The origin of Zn isotope fractionation in sulfides. Geochim. Cosmochim. Acta 75, 7632–7643.
Gagnevin, D., Boyce, A.J., Barrie, C.D., Menuge, J.F., Blakeman, R.J., 2012. Zn, Fe and S isotope fractionation in a large hydrothermal system. Geochim. Cosmochim. Acta 88, 183–198.
Gao, S., Yang, J., Zhou, L., Li, M., Hu, Z., Guo, J., Yuan, H., Gong, H., Xiao, G., Wei, J., 2011. Age and growth of the Archean Kongling terrain, South China, with emphasis on 3.3 Ga granitoid gneisses. Am. J. Sci. 311, 153–182.
Haest, M., Muchez, Ph., Petit, J.C.J., 2009. Cu isotope ratio variations in the Dikulushi Cu–Ag deposit, DRC: of primary origin or induced by supergene reworking? Econ. Geol. 104, 1055–1064.
Han, R.S., Liu, C.Q., Huang, Z.L., Ma, D.Y., Li, Y., Hu, B., Ma, G.S., Lei, L., 2004. Fluid inclusion of calcite and sources of ore-forming fluids in the Huize Zn–Pb–(Ag–Ge) district, Yunnan, China. Acta Geol. Sin. (Engl. Ed.) 78, 583–591.
Han, R.S., Liu, C.Q., Huang, Z.L., Chen, J., Ma, D.Y., Lei, L., Ma, G.S., 2007. Geological features and origin of the Huize carbonate-hosted Zn–Pb–(Ag) District, Yunnan, South China. Ore Geol. Rev. 31, 360–383.
Han, R.S., Liu, C.Q., Carranza, E.J.M., Hou, B.H., Huang, Z.L., Wang, X.K., Hu, Y.Z., Lei, L., 2012. REE geochemistry of altered tectonites in the Huize base-metal district, Yunnan, China. Geochem. Explor. Environ. Anal. 12, 127–146.
Hu, R.Z., Zhou, M.F., 2012. Multiple Mesozoic mineralization events in South China — an introduction to the thematic issue. Miner. Deposita 47, 579–588.
Huang, Z.L., Li, W.B., Chen, J., Han, R.S., Liu, C.Q., Xu, C., Guan, T., 2003. Carbon and oxygen isotope constraints on the mantle fluids join the mineralization of the Huize super-large Pb–Zn deposits, Yunnan Province, China. J. Geochem. Explor. 78/79, 637–642.
Huang, Z.L., Chen, J., Han, R.S., Li, W.B., Liu, C.Q., Zhang, Z.L., Ma, D.Y., Gao, D.R., Yang, H.L., 2004. Geochemistry and ore-formation of the Huize giant lead–zinc deposit, Yunnan, Province, China: discussion on the relationship between Emeishan Flood basalts and lead–zinc mineralization. Geological Publishing House, Beijing 1–204 (in Chinese).
Huang, Z.L., Li, X.B., Zhou, M.F., Li, W.B., Jin, Z.G., 2010. REE and C–O isotopic geochemistry of calcites from the world-class Huize Pb–Zn deposit, Yunnan, China: implications for the ore genesis. Acta Geol. Sin. (Engl. Ed.) 84, 597–613.
Ikeihata, K., Hirata, T., 2012. Copper isotope characteristics of copper-rich minerals from the Horoman peridotite complex, Hokkaido, northern Japan. Econ. Geol. 107, 1489–1497.
John, S.G., Rouxel, O.J., Craddock, P.R., Engwall, A.M., Boyle, E.A., 2008. Zinc stable isotopes in seafloor hydrothermal vent fluids and chimneys. Earth Planet. Sci. Lett. 269, 17–28.
Kelley, K.D., Wilkinson, J.J., Chapman, J.B., Crowther, H.L., Weiss, D.J., 2009. Zinc isotopes in sphalerite from base metal deposits on the Red Dog district, Northern Alaska. Econ. Geol. 104, 767–773.
Larson, P.B., Mather, K., Ramos, F.C., Chang, Z., Gaspar, M., Meinert, L.D., 2003. Copper isotope ratios in magmatic and hydrothermal ore forming environment. Chem. Geol. 201, 337–350.
Li, W.B., Huang, Z.L., Yin, M.D., 2007a. Isotope geochemistry of the Huize Zn–Pb ore field, Yunnan province, southwestern China: Implication for the sources of ore fluid and metals. Geochem. J. 41, 65–81.
Li, W.B., Huang, Z.L., Yin, M.D., 2007b. Dating of the giant Huize Zn–Pb ore field of Yunnan province, southwest China: constraints from the Sm–Nd system in hydrothermal calcite. Resour. Geol. 57, 90–97.
Li, S.Z., Zhu, X.K., Tang, S.H., He, X.X., Cai, J.J., 2008. The application of MC-ICP-MS to high-precision measurement of Zn isotope ratios. Acta Petrol. Mineral. 27, 273–278 (in Chinese with English abstract).
Lin, Z.Y., Wang, D.H., Zhang, C.Q., 2010. Rb–Sr isotopic age of sphalerite from the Paoma lead–zinc deposit in Sichuan Province and its implications. Geol. China 37, 196–488 (in Chinese with English abstract).
Liu, H.C., Lin, W.D., 1999. Study on the Law of Pb–Zn–Ag Ore Deposit in Northeast Yunnan, China. Yunnan University Press, Kunming 1–468 (in Chinese).
Machel, H.G., Krouse, H.R., Sassen, R., 1995. Products and distinguishing criteria of bacterial and thermochemical sulfate reduction. Appl. Geochem. 10, 373–389.
Maréchal, C.N., Sheppard, S.M.F., 2002. Isotopic fractionation of Cu and Zn between chloride and nitrate solutions and malachite or smithsonite at 30 °C and 50 °C. Goldschmidt Conference. Geochim. Cosmochim. Acta 66, A484.
Maréchal, C.N., Télouk, P., Albarède, F., 1999. Precise analysis of copper and zinc isotopic compositions by plasma-source mass spectrometry. Chem. Geol. 156, 251–273.
Markl, G., von Blanckenburg, F., Wagner, T., 2006. Iron isotope fractionation during hydrothermal ore deposition and alteration. Geochim. Cosmochim. Acta 70, 3011–3030.
Mason, T.F.D., Weiss, D.J., Horstwood, M., Parrish, R.R., Russell, S.S., Mullance, E., Coles, J.B., 2004a. High-precision Cu and Zn isotope analysis by plasma source mass spectrometry: Part 1 Spectral interferences and their correction. J. Anal. At. Spectrom. 19, 209–217.
Mason, T.F.D., Weiss, D.J., Horstwood, M., Parrish, R.R., Russell, S.S., Mullance, E., Coles, J.B., 2004b. High-precision Cu and Zn isotope analysis by plasma source mass spectrometry: part 2 correction for mass discrimination effects. J. Anal. At. Spectrom. 19, 218–226.
Mason, T.F.D., Weiss, D.J., Chapman, J.B., Wilkinson, J.J., Tessalina, S.G., Spiro, B., Horstwood, M.S.A., Spratt, J., Coles, B.J., 2005. Zn and Cu isotopic variability in the Alexandrinka volcanic-hosted massive sulphide (VHMS) ore deposit, Urals, Russia. Chem. Geol. 221, 170–187.

Mathur, R., Titley, S., Barra, F., Brantley, S., Wilson, M., Phillips, A., Munizaga, F., Maksaev, V., Vervoort, J., Hart, G., 2009. Exploration potential of Cu isotope fractionation in porphyry copper deposits. J. Geochem. Explor. 102, 1–6.
Mathur, R., Dendas, M., Titley, S., Phillips, A., 2010. Patterns in the copper isotope composition of minerals in porphyry copper deposits in Southwestern United States. Econ. Geol. 105, 1457–1467.
Mathur, R., Ruiz, J., Casselman, M.J., Megaw, P., van Egmond, R., 2012. Use of Cu isotopes to distinguish primary and secondary Cu mineralization in the Canariaco Norte porphyry copper deposit, northern Peru. Miner. Deposita 47, 755–762.
Muchez, P., Heijlen, W., Banks, D., Blundell, D., Boni, M., Grandia, F., 2005. Extensional tectonics and the timing and formation of basin-hosted deposits in Europe. Ore Geol. Rev. 27, 241–267.
Ohmoto, H., Goldhaber, M.B., 1997. Sulfur and carbon isotopes, In: Barnes, H.L. (Ed.), Geochemistry of Hydrothermal Ore Deposits, 3rd edition. Wiley, New York, pp. 517–611.
Ohmoto, H., Kaiser, C.J., Geer, K.A., 1990. Systematics of sulphur isotopes in recent marine sediments and ancient sediment-hosted base metal deposits. In: Herbert, H.K., Ho, S.E. (Eds.), Stable isotopes and Fluid Processes in Mineralisation, 23. Geol. Dep. Univ. Extens. Univ. Western Australia, pp. 70–120.
Qiu, Y.M., Gao, S., McNaughton, N.J., Groves, D.I., Ling, W.L., 2000. First evidence of >3.2 Ga continental crust in the Yangtze craton of south China and its implications for Archean crustal evolution and Phanerozoic tectonics. Geology 28, 11–14.
Reid, A., Wilson, C.J.L., Shun, L., Pearson, N., Belousova, E., 2007. Mesozoic plutons of the Yidun Arc, SW China: U/Pb geochronology and Hf isotopic signature. Ore Geol. Rev. 31, 88–106.
Rouxel, O., Fouquet, Y., Ludden, J.N., 2004. Copper isotope systematics of the Lucky Strike, Rainbow, and Logatchev sea-floor hydrothermal fields on the mid-Atlantic ridge. Econ. Geol. 99, 585–600.
Seal, I.R., 2006. Sulfur isotope geochemistry of sulfide minerals. Rev. Mineral. Geochem. 61, 633–677.
Sun, W.H., Zhou, M.F., Yan, D.P., Li, J.W., Ma, Y.X., 2009. Provenance and tectonic setting of the Neoproterozoic Yanbian Group, western Yangtze Block (SW China). Precambrian Res. 167, 213–236.
Tang, S.H., Zhu, X.K., Cai, J.J., Li, S.Z., He, X.X., Wang, J.H., 2006. Chromatographic separation of Cu, Fe and Zn using AG M P-1 anion exchange resin for isotope determination by MC-ICPMS. Rock Miner. Anal. 25, 5–8 (in Chinese with English abstract).
Toutain, J.P., Sonke, J., Munoz, M., Nonell, A., Polvé, M., Viers, J., Freydier, R., Sortino, F., Joron, J.L., Sumarti, S., 2008. Evidence for Zn isotopic fractionation at Merapi volcano. Chem. Geol. 253, 74–82.
Wang, W., Wang, F., Chen, F.K., Zhu, X.Y., Xiao, P., Siebel, W., 2010. Detrital zircon ages and Hf–Nd isotopic composition of Neoproterozoic sedimentary rocks in the Yangtze Block: Constraints on the deposition age and provenance. J. Geol. 118, 79–94.
Wang, Y., Zhu, X.K., Mao, J.W., Li, Z.H., Cheng, Y.B., 2011. Iron isotope fractionation during skarn-type metallogeny: a case study of Xinqiao Cu–S–Fe–Au deposit in the Middle–Lower Yangtze valley. Ore Geol. Rev. 43, 194–202.
Wang, W., Zhou, M.F., Yan, D.P., Li, J.W., 2012. Depositional age, provenance, and tectonic setting of the Neoproterozoic Sibao Group, southeastern Yangtze Block, South China. Precambrian Res. 192–195, 107–124.
Wilkinson, J.J., Weiss, D.J., Mason, T.F.D., Coles, B.J., 2005. Zinc isotope variation in hydrothermal systems: preliminary evidence from the Irish Midlands ore field. Econ. Geol. 100, 583–590.
Yan, D.P., Zhou, M.F., Song, H.L., Wang, X.W., Malpas, J., 2003. Origin and tectonic significance of a Mesozoic multi-layer over-thrust system within the Yangtze Block (South China). Tectonophysics 361, 239–254.
Zartman, R.E., Doe, B.R., 1981. Plumbotectonics — the model. Tectonophysics 75, 135–162.
Zhang, Z.B., Li, C.Y., Tu, G.C., Xia, B., Wei, Z.Q., 2006. Geotectonic evolution background and ore-forming process of Pb–Zn deposits in Chuan–Dian–Qian area of southwest China. Geotecton. Metallog. 30, 343–354 (in Chinese with English abstract).
Zhao, X.F., Zhou, M.F., Li, J.W., Sun, M., Gao, J.F., Sun, W.H., Yang, J.H., 2010. Late Paleoproterozoic to early Mesoproterozoic Dongchuan Group in Yunnan, SW China: implications for tectonic evolution of the Yangtze Block. Precambrian Res. 182, 57–69.
Zheng, M.H., Wang, X.C., 1991. Genesis of the Daliangzi Pb–Zn deposit in Sichuan, China. Econ. Geol. 86, 831–846.
Zhou, C.X., Wei, C.S., Guo, J.Y., 2001. The source of metals in the Qilingchang Pb–Zn deposit, Northeastern Yunnan, China: Pb–Sr isotope constraints. Econ. Geol. 96, 583–598.
Zhou, M.F., Yan, D.P., Kennedy, A.K., Li, Y.Q., Ding, J., 2002a. SHRIMP zircon geochronological and geochemical evidence for Neo-proterozoic arc-related magmatism along the western margin of the Yangtze Block, South China. Earth Planet. Sci. Lett. 196, 1–67.
Zhou, M.F., Malpas, J., Song, X.Y., Robinson, P.T., Sun, M., Kennedy, A.K., Lesher, C.M., Keays, R.R., 2002b. A temporal link between the Emeishan large igneous province (SW China) and the end-Guadalupian mass extinction Earth. Earth Planet. Sci. Lett. 196, 113–122.
Zhou, J.X., Huang, Z.L., Zhou, G.F., Li, X.B., Ding, W., Bao, G.P., 2011. Trace elements and rare earth elements of sulfide minerals in the Tianqiao Pb–Zn ore deposit, Guizhou province, China. Acta Geol. Sin. (Engl. Ed.) 85, 189–199.
Zhou, J.X., Huang, Z.L., Zhou, M.F., Li, X.B., Jin, Z.G., 2013a. Constraints of C–O–S–Pb isotope compositions and Rb–Sr isotopic age on the origin of the Tianqiao carbonate-hosted Pb–Zn deposit, SW China. Ore Geol. Rev. 53, 77–92.
Zhou, J.X., Huang, Z.L., Bao, G.P., 2013b. Geological and sulfur–lead–strontium isotopic studies of the Shaojiwan Pb–Zn deposit, southwest China: implications for the origin of hydrothermal fluids. J. Geochem. Explor. 128, 51–61.
Zhou, J.X., Huang, Z.L., Yan, Z.F., 2013c. The origin of the Maozu carbonate–hosted Pb–Zn deposit, southwest China: constrained by C–O–S–Pb isotopic compositions and Sm–Nd isotopic age. J. Asian Earth Sci. 73, 39–47.
Zhu, X.K., O'Nions, R.K., Guo, Y., Belshaw, N.S., Rickard, D., 2000. Determination of natural Cu isotope variation by plasmas source mass spectrometry: implications for use as geochemical tracers. Chem. Geol. 163, 139–149.
Zhu, X.K., Guo, Y., Williams, R.J.P., O'Nions, R.K., Matthews, A., Belshaw, N.S., Canters, G.W., Waal, E.C.D., Weser, U., Burgess, B.K., Salvato, B., 2002. Mass fractionation processes of transition metal isotopes. Earth Planet. Sci. Lett. 200, 47–62.